Article

Diversification of Self-Organized Architectures in Supramolecular Dye Assemblies

Shiki Yagai, Tetsuro Kinoshita, Masatsugu Higashi, Keiki Kishikawa, Takashi Nakanishi, Takashi Karatsu, and Akihide Kitamura

J. Am. Chem. Soc., **2007**, 129 (43), 13277-13287• DOI: 10.1021/ja075257c • Publication Date (Web): 05 October 2007

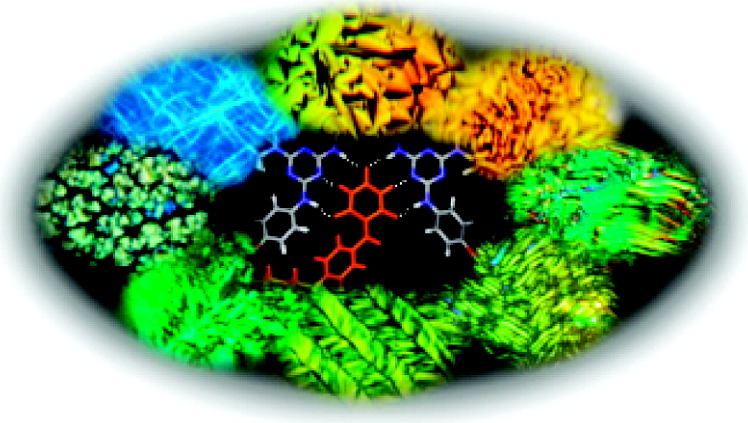

J|A|C|S
ARTICLES
Published on Web 10/05/2007

Diversification of Self-Organized Architectures in Supramolecular Dye Assemblies

Shiki Yagai,*,†,‡ Tetsuro Kinoshita,† Masatsugu Higashi,† Keiki Kishikawa,† Takashi Nakanishi,§ Takashi Karatsu,† and Akihide Kitamura†

Contribution from Department of Applied Chemistry and Biotechnology, Faculty of Engineering, Chiba University, 1-33 Yayoi-cho, Inage-ku, Chiba 263-8522, Japan, PRESTO, Japan Science and Technology Agency (JST), 4-1-8 Honcho Kawaguchi, Saitama, Japan, National Institute for Materials Science (NIMS), 1-2-1 Sengen, Tsukuba 305-0047, Japan, and Max Planck Institute of Colloids and Interfaces, Research Campus Golm, Potsdam 14424, Germany

Received July 14, 2007; E-mail: yagai@faculty.chiba-u.jp

Abstract: Upon complexation with bismelamine receptors (**BM*n***) featuring different alkyl linker lengths (number of methylene groups (*n*) = 5−12), a barbituric acid merocyanine dye (**1**) can be loaded into diverse self-organized superstructures through multiple hydrogen-bonding interactions. UV/vis, dynamic light scattering, and NMR studies in cyclohexane demonstrate that the diversification of the primarily formed hydrogen-bonded species in solution occurs by varying the linker length of **BM*n***. Hierarchical organization of the hydrogen-bonded species is achieved by slow evaporation of the solvent (forming solvent-free films), and the resulting superstructures are evaluated by polarized optical microscopy, X-ray diffraction, SEM, and AFM techniques. The formation of columnar structures with and without two-dimensional ordering are revealed for shorter (*n* = 5−7) and longer (*n* = 11, 12) linker bis(melamines), respectively. On the contrary, in the cases of *n* = 8−10, the formation of lamellar structures is unveiled. Several assemblies (*n* = 5, 7, 11) indicate the formation of a liquid crystalline mesophase in POM and DSC analyses. Hierarchical organization is also achieved in solution by prolonged aging, affording phase-separated crystalline nanofibers (*n* = 5, 7) and soft nanofibrils agglomerating into wormlike objects (*n* = 8), gel-forming continuous globular networks (*n* = 10), and nanofibers (*n* = 11, 12). These superstructural and morphological diversifications are an outcome of the variation in the primarily formed hydrogen-bonded supramolecular architectures. Using this strategy, diverse self-assembled materials will be obtained from a single dye component.

Introduction

Organic materials composed of supramolecularly organized functional dyes are essential for miniaturizing optoelectronic devices since they can be fabricated on the basis of the bottom-up approach.[1] Control of self-organized nano- to microarchitectures as well as local intermolecular electronic interactions are of primary importance as they determine electronic and optical properties of the materials.[2] Moreover, the generation of various material morphologies, such as liquids,[3] gels,[4] liquid crystals,[5] and discrete nanoobjects,[6] is also key to realize a broad range of practical applications. Thus, significant effort has been devoted to the systematic control and diversification of the self-assembled architectures of functional dyes with a minimum of synthetic modification.[7] However, systematic fabrication of diverse self-organized architectures and material morphologies from a single functional dye scaffold remains a challenging task for chemists, and most examples rely on synthetic modification

† Chiba University.
‡ PRESTO, JST.
§ National Institute for Materials Science and Max Planck Institute.

(1) (a) Schenning, A. P. H. J.; et al. *Synth. Met.* **2004**, *147*, 43−48. (b) Hoeben, F. J. M.; Jonkheijm, P.; Meijer, E. W.; Schenning, A. P. H. J. *Chem. Rev.* **2005**, *105*, 1491−1546. (c) Schenning, A. P. H. J.; Meijer, E. W. *Chem. Commun.* **2005**, 3245−3258.
(2) (a) Engelkamp, H.; Middelbeek, S.; Nolte, R. J. M. *Science* **1999**, *284*, 785−788. (b) Würthner, F. *Chem. Commun.* **2004**, 1564−1579. (c) Ajayaghosh, A.; George, S. J.; Schenning, A. P. H. J. *Top. Curr. Chem.* **2005**, *258*, 83−118. (d) Grimsdale, A. C.; Müllen, K. *Angew. Chem., Int. Ed.* **2005**, *44*, 5592−5629. (e) Elemans, J. A. A. W.; van Hameren, R.; Nolte, R. J. M.; Rowan, A. E. *Adv. Mater.* **2006**, *18*, 1251−1266.
(3) Michinobu, T.; Nakanishi, T.; Hill, J. P.; Funahashi, M.; Ariga, K. *J. Am. Chem. Soc.* **2006**, *128*, 10384−10385.
(4) (a) Terech, P.; Weiss, R. G. *Chem. Rev.* **1997**, *97*, 3133−3159. (b) Schoonbeek, F. S.; Van, Esch, J. H.; Wegewijs, B.; Rep, D. B. A.; De Haas, M. P.; Klapwijk, T. M.; Kellogg, R. M.; Feringa, B. L. *Angew. Chem., Int. Ed.* **1999**, *38*, 1393−1397. (c) Abdallah, D. J.; Weiss, R. G. *Adv. Mater.* **2000**, *12*, 1237−1247. (d) Ajayaghosh, A.; George, S. J. *J. Am. Chem. Soc.* **2001**, *123*, 5148−5149. (e) Ajayaghosh, A.; George, S. J.; Praveen, V. K. *Angew. Chem., Int. Ed.* **2003**, *42*, 332−335. (f) Würthner, F.; Yao, S.; Beginn, U. *Angew. Chem., Int. Ed.* **2003**, *42*, 3247−3250. (g) Kawano, S.-i.; Tamaru, S.-i.; Fujita, N.; Shinkai, S. *Chem.—Eur. J.* **2004**, *10*, 343−351. (h) Ishi-i, T.; Shinkai, S. *Top. Curr. Chem.* **2005**, *258*, 119−160. (i) Kishimura, A.; Yamashita, T.; Aida, T. *J. Am. Chem. Soc.* **2005**, *127*, 179−183. (j) Shirakawa, M.; Fujita, N.; Shinkai, S. *J. Am. Chem. Soc.* **2005**, *127*, 4164−4165. (k) Kitamura, T.; Nakaso, S.; Mizoshita, N.; Tochigi, Y.; Shimomura, T.; Moriyama, M.; Ito, K.; Kato, T. *J. Am. Chem. Soc.* **2005**, *127*, 14769−14775. (l) Del Guerzo, A.; Olive, A. G. L.; Reichwagen, J.; Hopf, H.; Desvergne, J.-P. *J. Am. Chem. Soc.* **2005**, *127*, 17984−17985. (m) Tanaka, S.; Shirakawa, M.; Kaneko, K.; Takeuchi, M.; Shinkai, S. *Langmuir* **2005**, *21*, 2163−2172. (n) George, S. J.; Ajayaghosh, A. *Chem.—Eur. J.* **2005**, *11*, 3217−3227. (o) Kawano, S.-i.; Fujita, N.; Shinkai, S. *Chem.—Eur. J.* **2005**, *11*, 4735−4742. (p) de Loos, M.; Feringa, B. L.; van Esch, J. H. *Eur. J. Org. Chem.* **2005**, 3615−3631. (q) Ajayaghosh, A.; Vijayakumar, C.; Varghese, R.; George, S. J. *Angew. Chem., Int. Ed.* **2006**, *45*, 456−460. (r) Ajayaghosh, A.; Vijayakumar, C.; Praveen, V. K.; Babu, S. S.; Varghese, R. *J. Am. Chem. Soc.* **2006**, *128*, 7174−7175. (s) Ajayaghosh, A.; Praveen, V. K.; Srinivasan, S.; Varghese, R. *Adv. Mater.* **2007**, *19*, 411−415.

of dye components. Here we present a unique system in which self-organized nano- to microarchitectures of functional dye assemblies can be diversified dramatically without synthetic modification of the dye component.

Supramolecular fabrication of functional dye assemblies based on directional multiple hydrogen-bonding interactions is a fascinating approach to create functional materials featuring highly organized dye architectures.[1,2b,8] According to this approach, naphthalene/perylene bisimides, oligo(*p*-phenylenevinylene), merocyanine assemblies, and even their coassemblies have been explored by the groups of Kimizuka and Kunitake,[9] Schenning and Meijer,[10] Würthner,[11] and others.[12] Recently we also reported supramolecular polymers[13] formed from a barbituric acid merocyanine dyes such as **1** and flexible bismelamine **BM12**[14] ($n = 12$ in Figure 1a) via complementary triple hydrogen-bonding interactions of a melamine−imide couple.[15−18] **BM12** formed organogels upon mixing with **1** in nonpolar solvents as a result of supramolecular polymerization. The most intriguing prospect of this type of studies is that optically and electronically active dye molecules can be easily incorporated into processable materials such as nanofibers, micelles, liquid crystals, organogels, and rather unique nano- to microobjects through the functionalization of dyes with multiple hydrogen-bonding sites. In this study our effort is devoted to the induction of these diverse material morphologies from the aforementioned **1**−bismelamine coassembly system without synthetic modification for the dye component.

Our strategy makes use of bismelamines **BM*n*** featuring different linker length ($n = 5-12$, Figure 1a) as binding partners of merocyanine **1** to produce different types of hydrogen-bonded supramolecular species such as a 1 + 1 so-called Hamilton-type complex[19] and extended or folded supramolecular polymers (Figure 1b).[20] If such different types of supramolecular species are indeed generated by varying the linker length of the bismelamine component, the resulting hydrogen-bonded species

(5) (a) Kato, T. *Struct. Bonding* **2000**, *96*, 95−146. (b) Sautter, A.; Thalacker, C.; Würthner, F. *Angew. Chem., Int. Ed.* **2001**, *40*, 4425−4428. (c) Kato, T.; Mizoshita, N.; Kanie, K. *Macromol. Rapid Commun.* **2001**, *22*, 797−814. (d) Percec, V.; et al. *Nature* **2002**, *419*, 384−387. (e) Sivakova, S.; Rowan, S. J. *Chem. Commun.* **2003**, 2428−2429. (f) Kato, T.; Mizoshita, N.; Kishimoto, K. *Angew. Chem., Int. Ed.* **2006**, *45*, 38−68. (g) Tan, B.-H.; Yoshio, M.; Ichikawa, T.; Mukai, T.; Ohno, H.; Kato, T. *Chem. Commun.* **2006**, 4703−4705.

(6) (a) Jin, L. Y.; Ahn, J.-H.; Lee, M. *J. Am. Chem. Soc.* **2004**, *126*, 12208−12209. (b) Hill, J. P.; Jin, W.; Kosaka, A.; Fujushima, T.; Ichihara, H.; Shimomura, T.; Ito, K.; Hashizume, T.; Ishii, N.; Aida, T. *Science* **2004**, *306*, 1481−1483. (c) Nakanishi, T.; Schmitt, W.; Michinobu, T.; Kurth, D. G.; Ariga, K. *Chem. Commun.* **2005**, 5982−5984. (d) Shklyarevskiy, I. O.; et al. *J. Am. Chem. Soc.* **2005**, *127*, 1112−1113. (e) Shimizu, T.; Masuda, M.; Minamikawa, H. *Chem. Rev.* **2005**, *105*, 1401−1443. (f) Kim, J.-K.; Lee, E.; Huang, Z.; Lee, M. *J. Am. Chem. Soc.* **2006**, *128*, 14022−14023. (g) Maeda, H.; Hasegawa, M.; Hashimoto, T.; Kakimoto, T.; Nishio, S.; Nakanishi, T. *J. Am. Chem. Soc.* **2006**, *128*, 10024−10025. (h) Zhang, X.; Chen, Z.; Würthner, F. *J. Am. Chem. Soc.* **2007**, *129*, 4886−4887. (i) Maeda, H.; Kusunose, Y.; Terasaki, M.; Ito, Y.; Fujimoto, C.; Fujii, R.; Nakanishi, T. *Chem. Asian J.* **2007**, *2*, 350−357.

(7) *Supramolecular Dye Chemistry*; Würthner, F., Ed.; Topics in Current Chemistry 258; Springer-Verlag: New York, 2005.

(8) Recent review of dye assemblies based on multiple hydrogen bonding interactions: Yagai, S. *J. Photochem. Photobiol., C: Photochem. Rev.* **2006**, *7*, 164−182.

(9) (a) Kimizuka, N.; Kawasaki, T.; Kunitake, T. *J. Am. Chem. Soc.* **1993**, *115*, 4387−4388. (b) Kimizuka, N.; Kawasaki, T.; Hirata, K.; Kunitake, T. *J. Am. Chem. Soc.* **1995**, *117*, 6360−6361. (c) Kimizuka, N.; Fujikawa, S.; Kuwahara, H.; Kunitake, T.; Marsh, A.; Lehn, J.-M. *J. Chem. Soc., Chem. Commun.* **1995**, 2103−2104. (d) Kimizuka, N.; Kawasaki, T.; Hirata, K.; Kunitake, T. *J. Am. Chem. Soc.* **1998**, *120*, 4094−4104.

(10) (a) Schenning, A. P. H. J.; Jonkheijm, P.; Peeters, E.; Meijer, E. W. *J. Am. Chem. Soc.* **2001**, *123*, 409−416. (b) El-Ghayoury, A.; Schenning, A. P. H. J.; Van Hal, P. A.; Van Duren, J. K. J.; Janssen, R. A. J.; Meijer, E. W. *Angew. Chem., Int. Ed.* **2001**, *40*, 3660−3663. (c) Jonkheijm, P.; Hoeben, F. J. M.; Kleppinger, R.; Van Herrikhuyzen, J.; Schenning, A. P. H. J.; Meijer, E. W. *J. Am. Chem. Soc.* **2003**, *125*, 15941−15949. (d) Hoeben, F. J. M.; et al. *Angew. Chem., Int. Ed.* **2004**, *43*, 1976−1979. (e) Dudek, S. P.; Pouderoijen, M.; Abbel, R.; Schenning, A. P. H. J.; Meijer, E. W. *J. Am. Chem. Soc.* **2005**, *127*, 11763−11768. (f) Hoeben, F. J. M.; Pouderoijen, M. J.; Schenning, A. P. H. J.; Meijer, E. W. *Org. Biomol. Chem.* **2006**, *4*, 4460−4462. (g) Janssen, P. G. A.; Vandenbergh, J.; Van Dongen, J. L. J.; Meijer, E. W.; Schenning, A. P. H. J. *J. Am. Chem. Soc.* **2007**, *129*, 6078−6079.

(11) (a) Würthner, F.; Thalacker, C.; Sautter, A. *Adv. Mater.* **1999**, *11*, 754−758. (b) Würthner, F.; Thalacker, C.; Sautter, A.; Schartl, W.; Ibach, W.; Hollricher, O. *Chem.−Eur. J.* **2000**, *6*, 3871−3886. (c) Würthner, F.; Yao, S.; Heise, B.; Tschierske, C. *Chem. Commun.* **2001**, 2260−2261. (d) Würthner, F.; Yao, S. *J. Org. Chem.* **2003**, *68*, 8943−8949. (e) Würthner, F.; et al. *J. Am. Chem. Soc.* **2004**, *126*, 10611−10618. (f) Würthner, F.; Schmidt, J.; Stolte, M.; Wortmann, R. *Angew. Chem., Int. Ed.* **2006**, *45*, 3842−3846.

(12) (a) Saadeh, H.; Wang, L.; Yu, L. *J. Am. Chem. Soc.* **2000**, *122*, 546−547. (b) Ilhan, F.; Gray, M.; Rotello, V. M. *Macromolecules* **2001**, *34*, 2597−2601. Goodman, A. J.; Breinlinger, E. C.; McIntosh, C. M.; Grimaldi, L. N.; Rotello, V. M. *Org. Lett.* **2001**, *3*, 1531−1534. (c) Yagai, S.; Monma, Y.; Kawauchi, N.; Karatsu, T.; Kitamura, A. *Org. Lett.* **2007**, *9*, 1137−1140.

(13) Supramolecular polymers based on multiple hydrogen-bonding interactions: (a) Fouquey, C.; Lehn, J. M.; Levelut, A. M. *Adv. Mater.* **1990**, *2*, 254−257. (b) Kotera, M.; Lehn, J. M.; Vigneron, J. P. *J. Chem. Soc., Chem. Commun.* **1994**, 197−199. (c) Koyano, H.; Bissel, P.; Yoshihara, K.; Ariga, K.; Kunitake, T. *Chem.−Eur. J.* **1997**, *3*, 1077−1082. (d) Sijbesma, R. P.; Beijer, F. H.; Brunsveld, L.; Folmer, B. J. B.; Hirschberg, J. H. K. K.; Lange, R. F. M.; Lowe, J. K. L.; Meijer, E. W. *Science* **1997**, *278*, 1601−1604. (e) Ariga, K.; Kunitake, T. *Acc. Chem. Res.* **1998**, *31*, 371−378. (f) Castellano, R. K.; Rebek, J., Jr. *J. Am. Chem. Soc.* **1998**, *120*, 3657−3663. (g) Moore, J. S. *Curr. Opin. Colloid Interface Sci.* **1999**, *4*, 108−116. (h) Choi, I. S.; Li, X.; Simanek, E. E.; Akaba, R.; Whitesides, G. M. *Chem. Mater.* **1999**, *11*, 684−690. (i) Klok, H.-A.; Jolliffe, K. A.; Schauer, C. L.; Prins, L. J.; Spatz, J. P.; Moeller, M.; Timmerman, P.; Reinhoudt, D. N. *J. Am. Chem. Soc.* **1999**, *121*, 7154−7155. (j) Gottarelli, G.; Masiero, S.; Mezzina, E.; Pieraccini, S.; Rabe, J. P.; Samori, P.; Spada, G. P. *Chem.−Eur. J.* **2000**, *6*, 3242−3248. (k) Brunsveld, L.; Folmer, B. J. B.; Meijer, E. W. *MRS Bull.* **2000**, *25*, 49−53. (l) Krische, M. J.; Lehn, J.-M. *Struct. Bonding* **2000**, *96*, 3−29. (m) Brunsveld, L.; Folmer, B. J. B.; Meijer, E. W.; Sijbesma, R. P. *Chem. Rev.* **2001**, *101*, 4071−4097. (n) Kanie, K.; Nishii, M.; Yasuda, T.; Taki, T.; Ujiie, S.; Kato, T. *J. Mater. Chem.* **2001**, *11*, 2875−2886. (o) Folmer, B. J.; Sijbesma, R. P.; Meijer, E. W. *J. Am. Chem. Soc.* **2001**, *123*, 2093−2094. (p) Kawasaki, T.; Tokuhiro, M.; Kimizuka, N.; Kunitake, T. *J. Am. Chem. Soc.* **2001**, *123*, 6792−6800. (q) Ciferri, A. *Macromol. Rapid Commun.* **2002**, *23*, 511−529. (r) Lehn, J.-M. *Polym. Int.* **2002**, *51*, 825−839. (s) Berl, V.; Schmutz, M.; Krische, M. J.; Khoury, R. G.; Lehn, J.-M. *Chem.−Eur. J.* **2002**, *8*, 1227−1244. (t) Giorgi, T.; Grepioni, F.; Manet, I.; Mariani, P.; Masiero, S.; Mezzina, E.; Pieraccini, S.; Saturni, L.; Spada, Gian, P.; Gottarelli, G. *Chem.−Eur. J.* **2002**, *8*, 2143−2152. (u) Yagai, S.; Iwashima, T.; Karatsu, T.; Kitamura, A. *Chem. Commun.* **2004**, 1114−1115. (v) Yagai, S.; Iwashima, T.; Kishikawa, K.; Nakahara, S.; Karatsu, T.; Kitamura, A. *Chem.−Eur. J.* **2006**, *12*, 3984−3994.

(14) (a) Yagai, S.; Higashi, M.; Karatsu, T.; Kitamura, A. *Chem. Mater.* **2004**, *16*, 3582−3585. (b) Yagai, S.; Higashi, M.; Karatsu, T.; Kitamura, A. *Chem. Mater.* **2005**, *17*, 4392−4398. (c) Yagai, S.; Karatsu, T.; Kitamura, A. *Langmuir* **2005**, *21*, 11048−11052.

(15) Calix[4]arene-bridged bismelamines have been used as building blocks for double-rosette molecular boxes and their higher-order assemblies: (a) Timmerman, P.; Vreekamp, R. H.; Hulst, R.; Verboom, W.; Reinhoudt, D. N.; Rissanen, K.; Udachin, K. A.; Ripmeester, J. *Chem.−Eur. J.* **1997**, *3*, 1823−1832. (b) Prins, L. J.; Huskens, J.; De Jong, F.; Timmerman, P.; Reinhoudt, D. N. *Nature* **1999**, *398*, 498−502. (c) Klok, H.-A.; Jolliffe, K. A.; Schauer, C. L.; Prins, L. J.; Spatz, J. P.; Möller, M.; Timmerman, P.; Reinhoudt, D. N. *J. Am. Chem. Soc.* **1999**, *121*, 7154−7155. (d) Prins, L. J.; Reinhoudt, D. N.; Timmerman, P. *Angew. Chem., Int. Ed.* **2001**, *40*, 2382−2426. (e) Timmerman, P.; Prins, L. J. *Eur. J. Org. Chem.* **2001**, 3191−3205. (f) Piermattei, A.; Giesbers, M.; Marcelis, A. T. M.; Mendes, E.; Picken, S. J.; Crego-Calama, M.; Reinhoudt, D. N. *Angew. Chem., Int. Ed.* **2006**, *45*, 7543−7546.

(16) (a) Zerkowski, J. A.; Seto, C. T.; Wierda, D. A.; Whitesides, G. M. *J. Am. Chem. Soc.* **1990**, *112*, 9025−9026. (b) Zerkowski, J. A.; Seto, C. T.; Whitesides, G. M. *J. Am. Chem. Soc.* **1992**, *114*, 5473−5475. (c) Zerkowski, J. A.; MacDonald, J. C.; Seto, C. T.; Wierda, D. A.; Whitesides, G. M. *J. Am. Chem. Soc.* **1994**, *116*, 2382−2391. (d) Zerkowski, J. A.; Whitesides, G. M. *J. Am. Chem. Soc.* **1994**, *116*, 4298−4304. (e) Zerkowski, J. A.; Mathias, J. P.; Whitesides, G. M. *J. Am. Chem. Soc.* **1994**, *116*, 4305−4315. (f) Mathias, J. P.; Simanek, E. E.; Zerkowski, J. A.; Seto, C. T.; Whitesides, G. M. *J. Am. Chem. Soc.* **1994**, *116*, 4316−4325. (g) Whitesides, G. M.; Simanek, E. E.; Mathias, J. P.; Seto, C. T.; Chin, D.; Mammen, M.; Gordon, D. M. *Acc. Chem. Res.* **1995**, *28*, 37−44.

(17) (a) Lehn, J. M.; Mascal, M.; DeCian, A.; Fischer, J. *J. Chem. Soc., Chem. Commun.* **1990**, 479−481. (b) Russell, K. C.; Leize, E.; Van, Dorsselaer, A.; Lehn, J.-M. *Angew. Chem., Int. Ed. Engl.* **1995**, *34*, 209−213. (c) Russell, K. C.; Lehn, J. M.; Kyritsakas, N.; DeCian, A.; Fischer, J. *New J. Chem.* **1998**, *22*, 123−128.

(18) For reviews of the supramolecular systems based on melamine−barbiturate/cyanurate hydrogen-bonding, see the following: (a) Lawrence, D. S.; Jiang, T.; Levett, M. *Chem. Rev.* **1995**, *95*, 2229−2260. (b) Sherrington, D. C.; Taskinen, K. A. *Chem. Soc. Rev.* **2001**, *30*, 83−93. (c) Archer, E. A.; Gong, H.; Krische, M. J. *Tetrahedron* **2001**, *57*, 1139−1159.

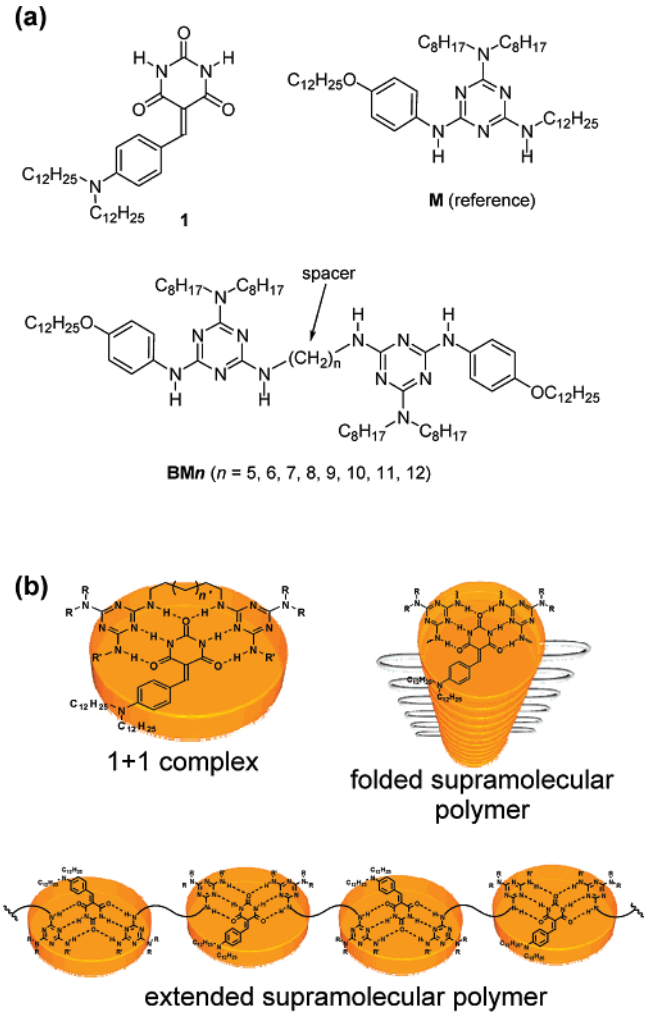

Figure 1. (a) Structure of merocyanine **1**, bismelamines **BM*n***, and reference monotopic melamine **M**. (b) Possible supramolecular species formed between **1** and **BM*n***.

would hierarchically self-organize in such a way that their morphologies are effectively introduced into the self-organizing process. This eventually leads to the diversification of self-organized dye architectures without any need for the structural alteration of the merocyanine dye. Thus, verification of this strategy will contribute to the development of a general way to obtain diverse nanoarchitectures and self-assembled materials from a single functional dye.

Results and Discussion

Solution Studies. Merocyanine **1** is a versatile functional molecule owing to its fruitful optical properties derived from electron donor−π-acceptor character as well as multiple hydrogen-bonding capability.[21] However, these structural properties make **1** insoluble in most nonpolar solvents such as cyclohexane and decane. The barbituric acid moiety of **1** has two acceptor−donor−acceptor (ADA) type triple hydrogen-bonding arrays that complementary bind to donor−acceptor−donor (DAD) type melamine modules. The 1:1 complexation of **1** with ditopic bismelamines (**BM*n***) is thus expected to afford various supramolecular species (**1·BM*n***) as shown in Figure 1b. Though the binding constants for this type of hydrogen-bonding interactions are relatively low (ca. 10^2 M^{-1}) in common organic solvents such as chloroform, strong binding can be achieved in nonpolar solvents such as cyclohexane ($K_a = 10^4-10^5$ M^{-1}).[11b] Thus, heating of **1** in the presence of an equimolar amount of **BM*n*** in cyclohexane gave homogeneous solutions, which do not form precipitates at least for a few days at room temperature even in high-concentration regime ($\sim 1.0 \times 10^{-2}$ M) where **1** precipitates immediately.

All the 1:1 mixtures of **1** and **BM*n*** in cyclohexane at concentration of 1.0×10^{-5} M show intramolecular charge-transfer bands of **1** at around $\lambda_{max} = 467-469$ nm. The absorption maxima are red-shifted from that of pure **1** in cyclohexane ($\lambda_{max} = 456$ nm), indicating the hydrogen-bonding interactions with **BM*n***. The spectra of all the mixtures show no significant change upon dilution up to 1.0×10^{-6} M. This is a notable feature for the complexation between **1** and ditopic **BM*n*** because the 2:1 complexation of **1** with a reference monotopic melamine **M** shows a clear transition from completely aggregated ($\lambda_{max} = 465$ nm) to monomeric state ($\lambda_{max} = 456$ nm) upon diluting the solution from 3.0×10^{-4} to 2.0×10^{-6} M (Figure S1). This finding implies the formation of Hamilton type 1 + 1 complex (Figure 1b) which is stabilized by the cooperative binding of the two melamine sites of **BM*n*** to **1** or the formation of $m + m$ ($m > 1$) cyclic oligomers[22] as shown in Figure S2. Attempt to detect such small assemblies in diluted solutions using dynamic light scattering (DLS) was hampered by low light scattering intensity. However, when cyclohexane solutions of **1·BM5−7** and **1·BM9** were condensed up to 7.5×10^{-3} M, reproducible autocorrelation functions that correspond to the average hydrodynamic diameters of 4.0−4.5 nm were detected (Figure 2). The 4 nm diameter is too small for the dimension of $m + m$ cyclic oligomers (6−7 nm in the case of 2 + 2 species) but in good agreement with the gyration diameters of the molecular-modeled 1 + 1 complexes with extended alkyl chains (Figure S4). In great contrast, **1·BM8** and **1·BM10** already start to form particles whose hydrodynamic diameters are polydispersed in the range of 5−40 nm for the former and 10−70 nm for the latter at a concentration of 1×10^{-3} M, indicating the formation of "open" polymeric species upon condensation (concentration-dependent polymerization).[23] This tendency is more pronounced for **1·BM11** and **1·BM12**, showing hydrodynamic diameters at around 100 nm even at

(19) (a) Hamilton, A. D.; Van Engen, D. *J. Am. Chem. Soc.* **1987**, *109*, 5035−5036. (b) Chang, S. K.; Hamilton, A. D. *J. Am. Chem. Soc.* **1988**, *110*, 1318−1319. (c) Tecilla, P.; Dixon, R. P.; Slobodkin, G.; Alavi, D. S.; Waldeck, D. H.; Hamilton, A. D. *J. Am. Chem. Soc.* **1990**, *112*, 9408−9410. (d) Tecilla, P.; Hamilton, A. D. *J. Chem. Soc., Chem. Commun.* **1990**, 1232−1234. (e) Chang, S.-K.; Van Engen, D.; Fan, E.; Hamilton, A. D. *J. Am. Chem. Soc.* **1991**, *113*, 7640−7645.
(20) ten Cate, A. T.; Sijbesma, R. P. *Macromol. Rapid Commun.* **2002**, *23*, 1094−1112.
(21) (a) Ahuja, R.; Caruso, P. L.; Moebius, D.; Paulus, W.; Ringsdorf, H.; Wildburg, G. *Angew. Chem., Int. Ed. Engl.* **1993**, *32*, 1033−1036. (b) Cao, Y. W.; Chai, X. D.; Chen, S. G.; Jiang, Y. S.; Yang, W. S.; Ren, Y. Z.; Blanchard-Desce, M.; Li, T. J.; Lehn, J.-M. *Synth. Met.* **1995**, *71*, 1733−1734. (c) Bohanon, T. M.; Denzinger, S.; Fink, R.; Paulus, W.; Ringsdorf, H.; Weck, M. *Angew. Chem., Int. Ed.* **1995**, *34*, 58−60. (d) Bohanon, T. M.; Caruso, P.-L.; Denzinger, S.; Fink, R.; Moebius, D.; Paulus, W.; Preece, J. A.; Ringsdorf, H.; Schollmeyer, D. *Langmuir* **1999**, *15*, 174−184. (e) Prins, L. J.; Thalacker, C.; Würthner, F.; Timmerman, P.; Reinhoudt, D. N. *Proc. Natl. Acad. Sci. U.S.A.* **2001**, *98*, 10042−10045. (f) Zhu, P.; Kang, H.; Facchetti, A.; Evmenenko, G.; Dutta, P.; Marks, T. J. *J. Am. Chem. Soc.* **2003**, *125*, 11496−11497. (g) Huang, X.; Li, C.; Jiang, S.; Wang, X.; Zhang, B.; Liu, M. *J. Am. Chem. Soc.* **2004**, *126*, 1322−1323.
(22) Lipkowski, P.; Bielejewska, A.; Timmerman, P.; Reinhoudt, D. N.; Kooijman, H.; Spek, A. L. *Chem. Commun.* **1999**, 1311−1312.
(23) (a) Ercolani, G.; Mandolini, L.; Mencarelli, P.; Roelens, S. *J. Am. Chem. Soc.* **1993**, *115*, 3901−3908. (b) Ercolani, G. *J. Phys. Chem. B* **1998**, *102*, 5699−5703. (c) Sontjens, S. H. M.; Sijbesma, R. P.; van Genderen, M. H. P.; Meijer, E. W. *Macromolecules* **2001**, *34*, 3815−3818.

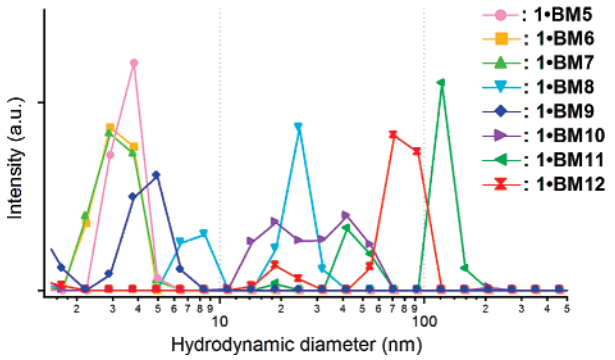

Figure 2. Hydrodynamic diameters in freshly prepared cyclohexane solutions of **1·BM*n*** analyzed by dynamic light scattering. Concentrations: 7.5×10^{-3} M for **1·BM5**, **1·BM6**, **1·BM7**, and **1·BM9**; 1×10^{-3} M for **1·BM8** and **1·BM10**; 2×10^{-4} M for **1·BM11** and **1·BM12**.

2.0×10^{-4} M. The considerably larger hydrodynamic diameters of **1·BM11** and **1·BM12** in comparison with those of **1·BM8** and **1·BM10** despite 5-fold dilution could be related to more efficient condensation-induced polymerization due to the longer linker moieties.

To gain more insight into the supramolecular species, ^{1}H NMR spectra of **1·BM*n*** were measured in cyclohexane-d_{12} at concentration of 5×10^{-3} M (Figure S5). Mixtures **1·BM5**, **1·BM6**, and **1·BM7** display relatively sharp resonances of the aromatic protons as well as the hydrogen-bonded protons of barbituric acid moiety of **1** at around 13−14 ppm, consistent with the formation of low-molecular-weight (Hamilton-type) complexes.[24] The spectrum of **1·BM9** is more broadened compared to the above three complexes, but the resonances of the hydrogen-bonded protons are visible. **1·BM8**, on the contrary, displays only a few broad signals in the aromatic region, suggesting that the assemblies are no longer low-molecular-weight species. It is interesting to note that the spectral resolution of **1·BM9** is higher than that of **1·BM8** despite its longer linker moiety, suggesting that degree of polymerization does not necessarily increase with the extension of the linker moiety. Above **1·BM10**, almost all aromatic proton resonances are hardly observed because of significant line broadening attributed to the formation of polymeric assemblies. These NMR results are fully consistent with the DLS results.

Hierarchical Organization of Hydrogen-Bonded Assemblies. When the complex solutions of **1·BM*n*** in cyclohexane ($c = 10^{-3}$−10^{-2} M) were dried on glass substrate, all the complexes gave birefringent crystalline films, ensuring the formation of highly ordered structures upon evaporation process. The IR spectra recorded from these solvent free films showed two major peaks assignable to the imide carbonyl stretching bands of **1** at around 1663−1670 and 1697−1713 cm^{-1}, which originally appeared as three peaks at 1646, 1673, and 1718 cm^{-1} for pure **1** (Figure S7). Similarly, the N−H stretching bands of pure **BM*n*** at 3413 and 3272 cm^{-1} shifted to 3333−3272 and 3220 cm^{-1} in the films, respectively. These IR spectral changes in hydrogen-bonding sites demonstrate the presence of hydrogen-bonding interactions different from those of pure **BM*n*** and **1**,[21g] thus confirming that **1** and **BM*n*** are in coassembled states through triple hydrogen-bonding interactions.

Table 1. Absorption Maxima of Solvent-free Films of **1·BM*n***

complex	λ_{max} (nm)	complex	λ_{max} (nm)
1·BM5	464	**1·BM9**	438
1·BM6	478	**1·BM10**	469
1·BM7	460	**1·BM11**	440
1·BM8	463	**1·BM12**	435

In contrast to diluted solutions, complexed films showed different absorption spectra for **1** (Table 1 and Figure S8), demonstrating merocyanine chromophores are indeed packed differently. The films of **1·BM5**, **1·BM7**, **1·BM8**, and **1·BM10** showed small shifts in maxima and significant line broadening as compared to diluted solutions, indicating the absence of specific chromophore orientations allowing strong excitonic coupling. An apparent red-shift was observed only for **1·BM6**, suggesting an offset stacking arrangement of **1**. On the other hand, the films of **1·BM9**, **1·BM11**, and **1·BM12** exhibited clear blue shifts indicating the H-type exciton coupling of merocyanine chromophores. The H-type exciton coupling in the films of **1·BM11** and **1·BM12** is important evidence of their unique morphologies which will be discussed later (see Folded Supramolecular Polymers section and ref 40). Fluorescence of **1** is strongly quenched in all the films except for **1·BM6**, due to dense chromophore packing or H-type exciton coupling. The fluorescence properties of **1·BM6** will be described in the next section.

The structural properties of these solvent-free materials were studied by polarized optical microscopy (POM) and X-ray diffraction (XRD). Furthermore, thermal behavior was investigated by using differential scanning calorimetry (DSC). These results are summarized in Table 2 and discussed in the following sections. Assemblies except for **1·BM6** and **1·BM9** hierarchically organize also in solution phase by aging to afford unique nanoscale objects, which were studied by optical microscopy (OM), field-emission scanning electron microscopy (FE-SEM), and atomic force microscopy (AFM).

1 + 1 Complexes. Solution-state studies provided strong evidence of the formation of Hamilton-type 1 + 1 complexes for **1·BM5**, **1·BM6**, **1·BM7**, and **1·BM9** in millimolar concentration regime. Such 1 + 1 complexes have discrete disklike shapes capable of organizing into columnar superstructures. When cyclohexane solutions of **1·BM5** were cast onto glass substrates and dried slowly under the atmosphere of cyclohexane at room temperature (ca. 1 day), birefringent circular textures were observed by POM (Figure 3a). Closer inspection of the individual circles by OM reveals that the ring nucleus were surrounded by circles (inset in Figure 3a), indicating the nonradial growth of the discotic entities. In contrast, **1·BM7** generates large spherulite textures shown in Figure 3b upon slow evaporation, indicating the radial growth of the discotic entities.

Upon heating, these textures abruptly turned into almost identical fan-shape textures characteristic of columnar liquid-crystalline phases around 65 °C (Figure 3c,d). DSC analysis indeed showed endothermic peaks at 62 °C ($\Delta H = 26.3$ kJ mol^{-1}) for **1·BM5** and at 63 °C ($\Delta H = 19.1$ kJ mol^{-1}) for **1·BM7** upon heating, indicating the formation of thermotropic liquid crystals (Table 2). These textures disappeared at around 70 °C upon further heating, where DSC showed endothermic

(24) Despite well-resolved ^{1}H NMR spectra of these complexes, titration experiments could not be carried out in this solvent due to insufficient solubility of free **1** (≈1.0×10^{-5} M). For **1·BM5**−**7**, titration experiments were thus carried out under diluted conditions using UV/Vis spectroscopy, affording well-defined binding isotherms indicative of 1:1 complexation with binding constant $K > 10^8$ M^{-1} (see Figure S6).

Table 2. XRD and DSC Data for Solvent-free Films of **1·BM*n***

complex	packing motif[a]	lattice param[b]	*d*-spacing[b] (Miller index)	phase transition and temp (enthalpy)[c]
1·BM5[d]	Col_h	$a = 25.4$	22.1 (100) 12.4 (110) 11.2 (200)	C → L; 62 (26.3) L → I; 70[e]
1·BM6[d]	Col_r	$a = 46.8/43.4$[f] $b = 24.5/27.8$[f]	23.4 (200 or 110) 21.7 (110 or 200)	C → I; 63 (31.7)
1·BM7[d]	Col_h[g]	$a = 28.7$	24.9 (100) 12.8 (200)	C → L; 63 (19.1) L → I; 75 (7.1)
1·BM8[d]	L	$c = 41.0$	40.8 (001) 33.7[h] 29.6[h] 23.2[h] 20.5 (002) 17.2[h] 15.1[h] 13.8 (003)	C → I; 65 (10.1)
1·BM9	L	$c = 37.1$	37.1 (001) 18.6 (002) 12.4 (003) 9.35 (004) 7.43 (005)	C → I; 72 (34.6) C ← I; 61 (6.0)
1·BM10	L	$c = 37.2$	37.2 (001) 18.1 (002) 12.0 (003)	C → I; 137 (25.3) C ← I; 121 (23.4)
1·BM11	Col	$a = 23.4$	23.4 14.8[h]	C → L; 131 (10.1) L → I; 144 (6.4) L ← I; 125 (4.2) C ← L; 112 (10.8)
1·BM12	Col	$a = 26.0$	26.0	C → I; 151 (30.3) C ← I; 140 (29.2)

[a] Col_h = hexagonal columnar packing, Col_r = rectangular columnar packing, L = lamellar packing, and Col = columnar packing possessing only orientational order. [b] *d*-spacings (Å) and lattice parameters (Å) were determined by XRD at 25 °C. [c] Phase transition temperatures (°C) and corresponding enthalpies (kJ/mol) were determined by DSC upon first heating (→) and cooling scan (←); C, crystalline phase; L, liquid crystalline phase; I, isotropic phase. [d] No phase transition was observed upon first cooling scan. [e] Enthalpy value could not be determined due to the overlap with the neighboring peak. [f] Lattice parameters can be calculated as two patterns due to the lack of higher-order reflections. [g] Despite the lack of (110) reflection, Col_h packing is strongly suggested from POM and DSC results almost identical with those of **1·BM5**. [h] Unidentified small peaks.

peaks at around 70 °C for **1·BM5**[25] and at 75 °C ($\Delta H = 7.1$ kJ mol^{-1}) for **1·BM7**. On cooling of the isotropic melts, the fan-shape textures no longer appeared and DSC showed no phase transition. These observations reveal that the melting of these complexes is accompanied by the breaking of (Hamilton-type) complex structures, which do not re-form via solid-state complexation.

XRD of the films of **1·BM5** showed a strong small-angle reflection at 22.1 Å with higher order reflections at $d = 12.4$ and 11.2 Å (Figure 3e), which can be assigned to the hexagonal columnar packing with a lattice parameter $a = 25.4$ Å. The small lattice parameter clearly excludes the organization of $m + m$ ($m > 1$) cyclic oligomers (see Figure S2). It is reasonable value when considering the dimension of the 1 + 1 complex (4.0 nm) with interdigitation of the exterior alkyl chains. The film of **1·BM7**, on the other hand, showed a strong reflection at 24.9 Å followed by a weak reflection at around 12.7 Å (Figure 3f). A definite assignment of the packing motif in this system cannot be made by XRD in the absence of unequivocal higher order reflections. Nonetheless, its thermal behavior as well as POM texture almost identical with those of **1·BM5** in addition to the fiber formation described below suggests a hexagonal columnar packing of this system with a lattice parameter $a = 28.7$ Å. The longer lattice parameter compared to **1·BM5** might be due to a marginal morphological difference between the two 1 + 1 complexes (vide infra). Thus, it is concluded that these disklike 1 + 1 complexes self-organize into hexagonally arranged columnar architectures with intercolumnar distance of ca. 25−29 Å.

The trend of **1·BM5** and **1·BM7** to self-organize into columnar structures is further highlighted by their organization behavior in solution. Aging the complex solutions of **1·BM5** and **1·BM7** in cyclohexane ($c = 5 \times 10^{-3}$ M) over weeks resulted in the formation of high-aspect ratio nanofibers with lengths reaching several hundreds of micrometers (Figure 4a,b). The fiber formation is likely to be a recrystallization process as no soluble extended assemblies were detected by DLS before precipitation. In decane, fiber formation progresses by hours with quantitative yield as judged by UV/vis absorption measurement of the mother liquids. Comparison of OM and POM images (Figure 4a−d) reveals that the fibers parallel either to the polarizer or analyzer (for example those indicated by arrows) are not visible under crossed-polarizer condition, indicating the uniaxial nature of the fibers. FE-SEM imaging revealed that the fibers are composed of bundled thinner fibers (spaghetti-like) with diameters less than 100 nm (Figures 4e and S9a). Cross-sectional images showed that the narrower fibers possess a solid interior (Figures 4f and S9b). These nanofibers gave XRD peaks almost identical with those of the films, indicating that the fibers consist of hexagonally packed columns of disklike 1 + 1 complexes. The formation of such high-quality nanofibers from structurally ill-defined (flexible) supramolecular building blocks is a striking consequence of molecular-recognition-directed self-assembly and hierarchical organization of the resulting supramolecular species.

(25) The enthalpy value could not be estimated because of the overlap with the peak corresponding to crystal−LC transition at 62 °C.

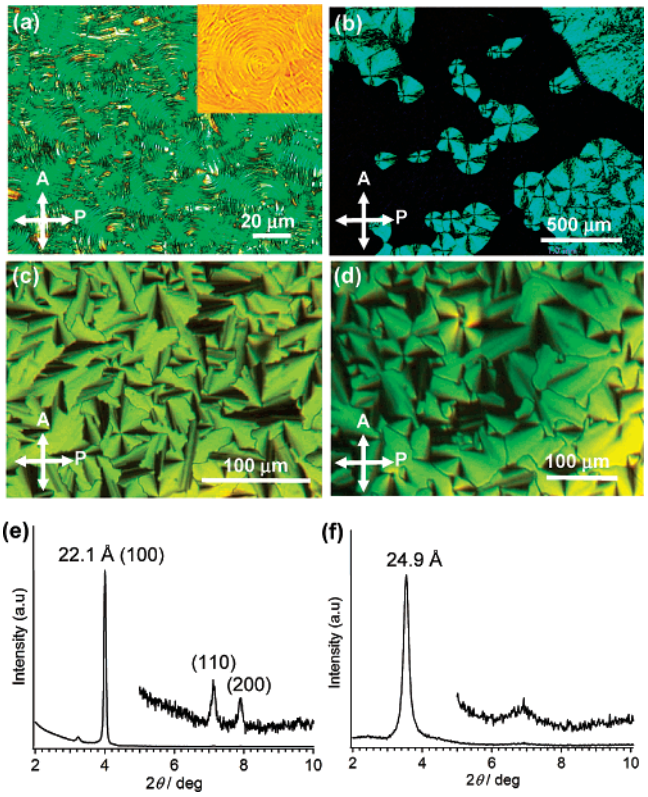

Figure 3. POM textures of solvent free films of **1·BM5** (a, c) and **1·BM7** (b, d) prepared by slow evaporation of cyclohexane solutions ($c = 5.0 \times 10^{-3}$ M). Images a and b were taken at 30 °C, and images c and d were taken at 70 °C. XRD patterns are shown of the solvent-free films of **1·BM5** (e) and **1·BM7** (f) at 70 °C. The inset in (a) is a magnified OM image of a circle.

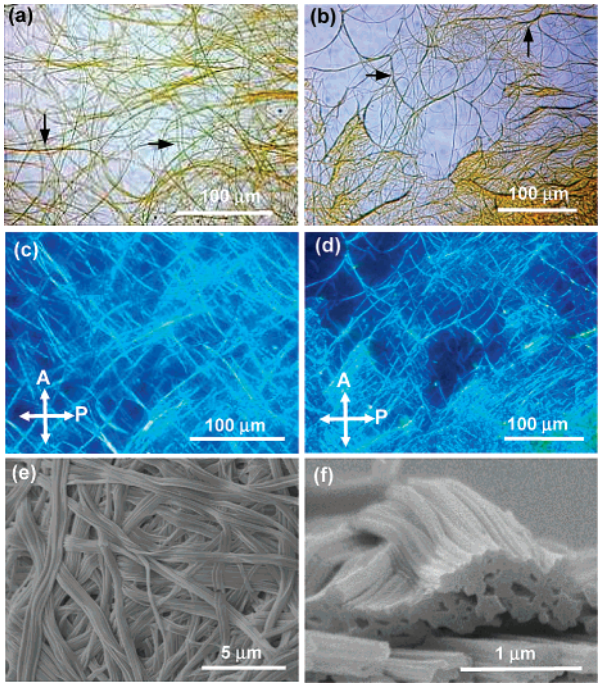

Figure 4. OM (a, b) and the corresponding POM images (c, d) of the nanofibers of **1·BM5** (a, c) and **1·BM7** (b, d) grown from cyclohexane solutions ($c = 5.0 \times 10^{-3}$ M) and SEM images of the nanofibers of **1·BM7** (e, f).

The mixture **1·BM6** shows self-organization behavior somewhat different from those of **1·BM5**/**7** despite the DLS and ^{1}H NMR characteristics ensuring the formation of 1 + 1 complex. Although the solvent-free film of this complex exhibits a fanlike birefringent texture even at room temperature, their extinction brushes rotated 37° with respect to the polarizer or analyzer (Figure 5a). This implies that the disks stack with a horizontal offset and that the disk planes are tilted at an angle 37° with respect to the normal of the column axis, leading to formation of a column with an ellipsoidal cross section. The film indeed shows two intense XRD peaks at 23.4 and 21.7 Å (Figure 5b), characteristic of the rectangular columnar packing arrangement favored by ellipsoidal columns. Because of the lack of the higher order reflections, we cannot determine the definite packing arrangement for this system. However, lattice parameters could be calculated as either $a = 46.8$ Å and $b = 24.5$ Å or $a = 43.4$ Å and $b = 27.8$ Å assuming the two small-angle peaks to be a combination of (200) and (110) reflections from a rectangular lattice with a $C2/m$ space group, respectively.

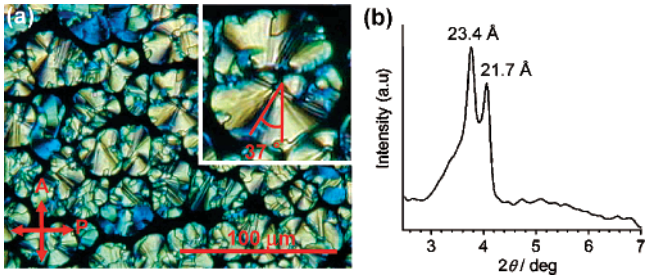

Figure 5. POM texture (a) and XRD pattern (b) of a solvent-free film of **1·BM6** prepared by slow evaporation of cyclohexane solution ($c = 5.0 \times 10^{-3}$ M).

This complex melted at 63 °C ($\Delta H = 31.7$ kJ mol^{-1}) without the formation of liquid-crystalline state as revealed by DSC (Table 2) and POM. The higher ΔH value of **1·BM6** compared to that of **1·BM5**/**7** might be due to the direct transition from crystalline phase to isotropic phase. For the same reason mentioned for **1·BM5**/**7**, the columnar structure does not appear upon cooling from the isotropic melt. As a striking consequence of the offset stacking arrangement of this complex, no phase-separated nanoobjects were generated from the solution phase by prolonged aging.[26]

Another striking consequence arising from the different stacking arrangements between **1·BM5**/**7** and **1·BM6** is their quite distinct optical properties of merocyanine **1**. UV/vis spectra of the films of **1·BM5**−**1·BM7** can be compared in Table 1 and Figure S8. These three films show relatively small spectral changes from the diluted solutions despite their highly ordered columnar packing. This indicates that the transition dipole moments of **1** within the columns lack a specific orientation as in conventional H- or J-aggregates and adopt random rotational displacements around the column axis.[27,28] Nonetheless, one important difference should be noted: the films of **1·BM5** and **1·BM7** showed almost identical spectra which are broadened and blue-shifted (~8 nm) compared to diluted cyclohexane solutions whereas the film of **1·BM6** showed a red-shift of 10 nm. Although these spectral shifts are too small to substantiate

(26) Similar result was obtained for hydrogen-bonded rosettes; see the following: Yagai, S.; Nakajima, T.; Kishikawa, K.; Kohmoto, S.; Karatsu, T.; Kitamura, A. *J. Am. Chem. Soc.* **2005**, *127*, 11134−11139.
(27) Rosch, U.; Yao, S.; Wortmann, R.; Würthner, F. *Angew. Chem., Int. Ed.* **2006**, *45*, 7026−7030.
(28) This is why these complexes adopt hexagonal columnar packing despite their nonsymmetrical shapes.

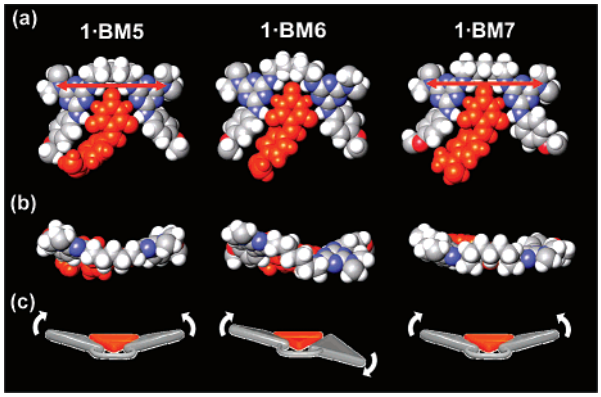

Figure 6. Energy-minimized structures of Hamilton-type 1 + 1 complexes of **1·BM5**−**1·BM7** (MacroModel ver. 9.0, OPLS force field). Long alkyl chains are omitted for clarity. Merocyanine **1** is shown in orange. Key: (a) top views; (b) horizontal views; (c) schematic representations highlighting geometrical difference. Red arrows in the top views of **1·BM5** and **1·BM7** correspond to the distance between the nitrogen atoms of the two dioctylamino groups (13.9 and 14.6 Å, respectively). Curved arrows in the schematic representations indicate the bending direction of the melamine plane from the coplanar arrangement to the barbiturate plane.

specific chromophore packing arrangements such as H- or J-type, the observed difference between **1·BM5/7** and **1·BM6** is consistent with the arguments made by POM and XRD studies in the sense that the latter complex takes more staggered stacking arrangement compared to the formers. This point can be more impressively demonstrated by the prominent red fluorescence observed only for the film of **1·BM6** upon UV irradiation (Figure S10a). The fluorescence spectrum of the film showed an broad emission peaked at 628 nm (Figure S10b), assignable to excimer-like species of **1** from its large Storks shift (5004 cm^{-1}).[29,30] A looser supramolecular packing in comparison with those of **1·BM5/7** probably allows structural reorganization required for the excimer formation.

Molecular modeling calculation was used to explain how marginal structural alterations in the linker length of the 1 + 1 complexes have a great impact on their packing arrangements. We searched a conformation of the alkyl linkers of **BM5**−**7** suitable for Hamilton-type receptor and found that conformations shown in Figure S3 are only possible ones. Force-field energy-minimization of these conformers bound to **1** provided reasonable 1 + 1 complexes for all the combinations as shown in Figure 6 parts a (top view) and b (front view). The most important feature here is their nonplanar structures, which might be due to the geometrical constraints of the two melamine planes imposed by the alkyl linkers. In the cases of **1·BM5** and **1·BM7**, two melamine planes bend disrotatorily with respect to **1** at the "triple hydrogen-bond hinges" due to the odd numbered oligomethylene linkers, resulting in the boatlike geometries (Figure 6c).[31] Deviation from planarity is apparently larger in **1·BM5** than in **1·BM7** (angles between the two melamine planes are 142 and 153°, respectively) because of the shorter linker length, leading to the shorter distance between the nitrogen atoms of the two dioctylamino groups in the former (13.9 Å) than in the latter (14.6 Å) (red arrows in Figure 6a). This is qualitatively consistent with the shorter intercolumnar distance of **1·BM5** (25.4 Å) than that of **1·BM7** (28.7 Å) revealed by XRD. On the other hand, the structure of **1·BM6** is characterized by conrotatorily bent two melamine planes due to the even numbered hexamethylene linker (Figure 6c). As a result, **1·BM6** shows a twisted chairlike geometry. Face-to-face stacking arrangement is evidently favored by symmetrical boatlike geometries of **1·BM5/7** but is disfavored by the contorted chairlike morphology of **1·BM6** due to the steric hindrance between the melamine moieties on stacking.

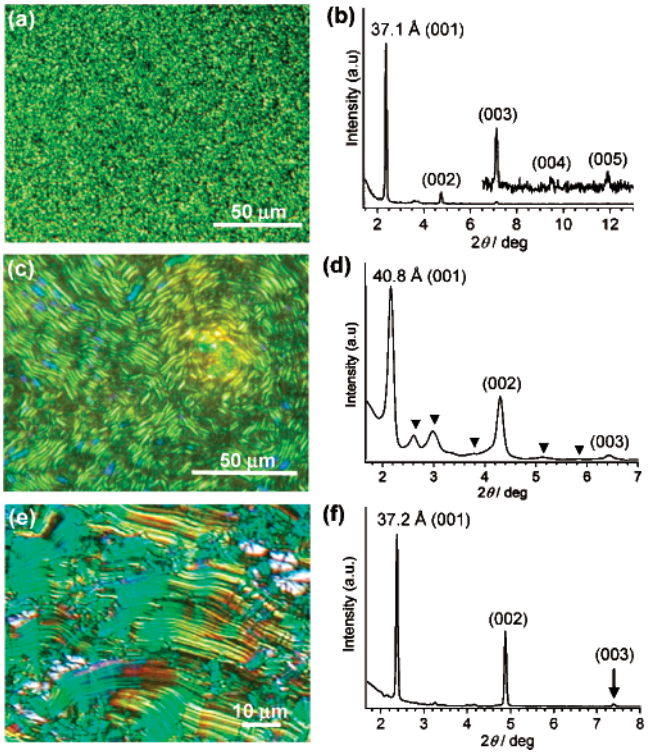

Figure 7. POM texture (a, c, e) and XRD pattern (b, d, f) of solvent-free films of **1·BM9** (a, b), **1·BM8** (c, d), and **1·BM10** (e, f) prepared by slow evaporation of cyclohexane solutions ($c = 5.0 \times 10^{-3}$ M).

Extended Supramolecular Polymers. The formation of a Hamilton-type 1 + 1 complex that is stable up to condensed state (film state) does not hold true when the number of carbon atoms in the linker moiety reaches 8. Thus, the complexation of **1** with **BM*n*** possessing middle linker length ($n = 8-10$) affords quasi-one-dimensional supramolecular polymers which hierarchically organize into lamellar superstructures. However, their self-organization propensities are different from each other as described below.

Combination of **1** and **BM9** shows a complicated self-organization behavior. As demonstrated by DLS, this mixture in cyclohexane exists as 1 + 1 complex at millimolar regime ($\sim 1.5 \times 10^{-2}$ M). The POM texture of the solvent-free film prepared by slow evaporation is, however, not fanlike as observed for discotic **1·BM5**−**1·BM7** but sandlike as observed for smectic phases of several liquid crystalline polymers (Figure 7a).[32] This implies the occurrence of major structural transition

(29) Zhu, W.; Pan, X.; Tian, H. *Synth. Met.* **2003**, *137*, 1127−1128.
(30) Aggregation-induced excimer formation has been reported for hydrogen-bonded assemblies. For example, see the following: (a) Ikeda, M.; Takeuchi, M.; Shinkai, S. *Chem. Commun.* **2003**, 1354−1355. (b) Yagai, S.; Higashi, M.; Karatsu, T.; Kitamura, A. *Chem. Commun.* **2006**, 1500−1502.
(31) Xiao, S.; Myers, M.; Miao, Q.; Sanaur, S.; Pang, K.; Steigerwald, M. L.; Nuckolls, C. *Angew. Chem., Int. Ed.* **2005**, *44*, 7390−7394.
(32) (a) Arehart, S. V.; Pugh, C. *J. Am. Chem. Soc.* **1997**, *119*, 3027−3037. (b) Hempenius, M. A.; Lammertink, R. G. H.; Vancso, G. J. *Macromolecules* **1997**, *30*, 266−272. (c) Busson, P.; Oertegren, J.; Ihre, H.; Gedde, U. W.; Hult, A.; Andersson, G.; Eriksson, A.; Lindgren, M. *Macromolecules* **2002**, *35*, 1663−1671.

upon evaporation process. This birefringent texture disappeared at around 70 °C upon heating without the indication for the formation of liquid crystalline phase, where DSC shows only one broad endothermic peak at 72.3 °C upon heating and an exothermic peak at 61 °C upon subsequent cooling from the isotropic phase. Surprisingly, the XRD of the film shows an intense, sharp small-angle reflection at 37.1 Å, which is accompanied by a number of weak reflections satisfying a reciprocal spacing ratio of 1:2:3:4:5 (Figure 7b). This substantiates the formation of a lamellar superstructure with a layer spacing of 37.1 Å. The formation of lamellar structures with longer interlayer distance compared to the intercolumnar distances of **1·BM5**/**7** clearly excludes the formation of discotic 1 + 1 complex in the solvent-free state and strongly suggests that the constituent supramolecular species in this system are extended tapelike supramolecular polymers (Figure 1b). Therefore, a model for this system includes the formation of 2-dimensional sheets by lateral organization of extended supramolecular polymers, which further accumulate to form lamellar superstructures. Since the 1 + 1 species of **1·BM9** should be unstable relative to those of **1·BM5**−**1·BM7** because of the conformational freedom associated with the nonamethylene linker, they open to form extended polymeric species upon increasing concentration (>1.5 × 10^{-2} M), resulting in the formation of lamellar superstructures. Because of this complicated behavior associated with cyclization−polymerization equilibrium, self-organization in cyclohexane does not proceed for this combination.[33]

In contrast to **1·BM9**, DLS studies of **1·BM8** and **1·BM10** indicate the formation of polydisperse supramolecular polymers in the solution state (Figure 2). At this stage, it becomes obvious that **BM*n*** possessing an odd number of carbon atoms in the linker moiety can form stable 1 + 1 species with **1**. When cyclohexane solutions of **1·BM8** and **1·BM10** were dried on glass substrate, the resultant solvent-free films exhibited characteristic textures as shown in Figure 7c,e, respectively. The texture of **1·BM8** is wormlike whereas that of **1·BM10** features many streaks reminiscent of lamellar structures. These textures manifest the capability of these supramolecular polymers to organize into highly ordered superstructures. Both **1·BM8** and **1·BM10** simply melted at 65 °C (ΔH = 10.1 kJ mol^{-1}) and 137 °C (ΔH = 25.3 kJ mol^{-1}), respectively, as examined by POM and DSC (Table 2). Significantly higher melting temperature of **1·BM10** may reflect a higher degree of polymerization as already suggested by DLS. **1·BM10** crystallized at 121 °C whereas **1·BM8** showed no phase transition upon cooling.

Despite the dramatic difference in POM textures, XRD revealed that fundamental organized structures of **1·BM8** and **1·BM10** are the same as that of **1·BM9**. Both the films feature intense three reflections indicating a lamellar ordering with the layer spacing of 40.8 Å for **1·BM8** and 37.2 Å for **1·BM10**, respectively (Figure 7d,f). For **1·BM8**, however, additional small reflections are observed at 33.7, 29.6, 23.2, 17.2, and 15.1 Å (marked by ▼), which can be indexed as (200), (110), (210), (400), and (410) reflections of rectangular columnar (Col_r) ordering with lattice parameters of a = 59.2 Å and b = 41.0 Å. A model for the organization of **1·BM8** thus may include

(33) In decane, this complex (c = 2.0 × 10^{-3} M) formed rigid gels upon aging for 1 month, indicating that polymerization occurs in this solvent. Similar solvent-induced polymerization has been reported for ureidopyrimidinone supramolecular polymers: see ref 39d.

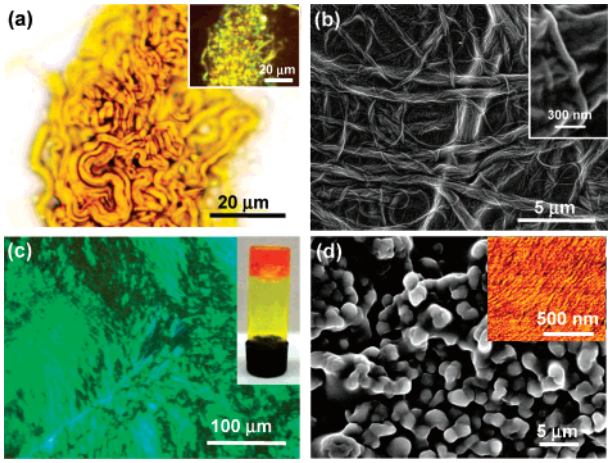

Figure 8. (a) Optical microscopic images of the wormlike objects of **1·BM8** grown from cyclohexane solution (c = 5.0 × 10^{-3} M). The inset shows the corresponding POM image. (b) FE-SEM images of the wormlike objects of **1·BM8**. The inset displays a thinner fibril. (c) POM image and appearance (inset) of a cyclohexane gel of **1·BM10** (5 × 10^{-3} M). (d) FE-SEM image of the xerogel of **1·BM10**. The inset shows the AFM phase image of the surface of a globular object.

lateral organization of extended supramolecular polymers to the 2-dimensional sheets with in-plane rectangular ordering of hydrogen-bonded disk segments.

Self-organization of supramolecular polymers **1·BM8** and **1·BM10** occurs also in solution by aging for a long time, affording unique nanoscopic objects. In the case of **1·BM8**, aging the cyclohexane solution (c = 1 × 10^{-2} M) for 1 month resulted in the precipitation of unique wormlike birefringent objects of 1−3 μm width and 20−400 μm length (Figure 8a). The use of decane as solvent promotes its formation within a few days. The strong birefringence indicates the crystalline packing of the supramolecular polymers. In several parts thinner fibrils with *several hundreds of micrometers* in length can be seen (Figure S11). FE-SEM imaging confirmed the presence of thinner fibrils with a uniform diameter of 100 nm (Figure 8b), leading to a high aspect ratio of >1000. In some parts wormlike objects are loosened to a number of thinner fibrils (Figure S12c), manifesting a hierarchical relationship between them. The fibrils are seemingly soft, which is in sharp contrast to the rigid nanofibers obtained from **1·BM5**/**7**. With a similar XRD pattern to that of the thin film (Figure 7d), we assume that such fibrils are formed by rolling up of the lamellae as proposed for bilayered amphiphilic glucoamide derivatives.[34]

On the contrary, the organization of **1·BM10** in cyclohexane resulted in gelation at concentrations above 2 × 10^{-3} M (0.5 wt %) after 1 month (inset in Figure 8c),[35] reiterating a higher degree of polymerization in this system. The use of decane as solvent promotes the gelation within a few days. The resulting gels are strongly birefringent (Figure 8c), indicating that the polymeric species assemble anisotropically in the presence of solvent molecules (formation of lyotropic mesophase). This characteristic property highlights the strong interchain associa-

(34) Fuhrhop, J. H.; Schnieder, P.; Boekema, E.; Helfrich, W. *J. Am. Chem. Soc.* **1988**, *110*, 2861−2867.

(35) For organogels based on the melamine−cyanurate/barbiturate motif, see the following: (a) Hanabusa, K.; Miki, T.; Taguchi, Y.; Koyama, T.; Shirai, H. *J. Chem. Soc., Chem. Commun.* **1993**, 1382−1384. (b) Inoue, K.; Ono, Y.; Kanekiyo, Y.; Ishi-i, T.; Yoshihara, K.; Shinkai, S. *J. Org. Chem.* **1999**, *64*, 2933−2937. (c) Jeong, S. W.; Murata, K.; Shinkai, S. *Supramol. Sci.* **1996**, *3*, 83−86. Also see ref 14.

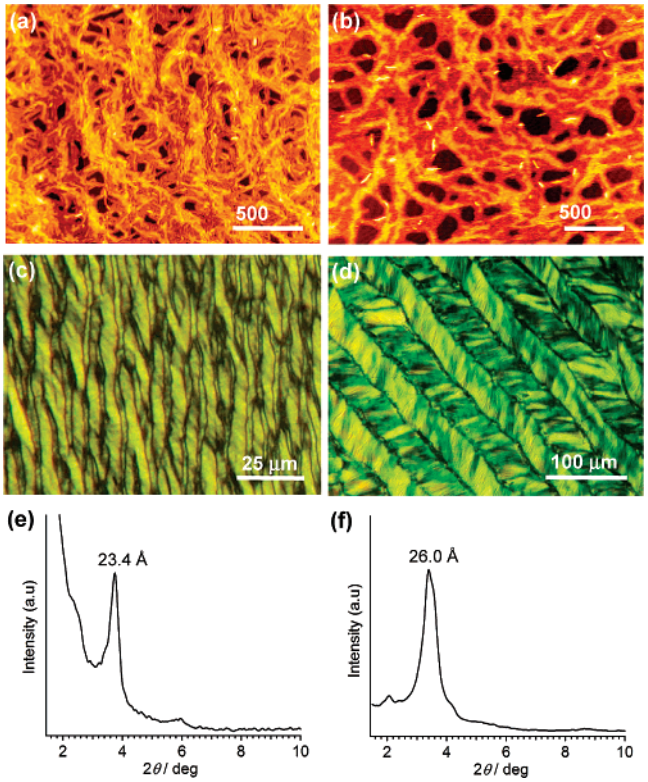

Figure 9. (a, b) AFM height images of spin-coated cyclohexane solutions ($c = 2 \times 10^{-4}$ M) of **1·BM11** (a) and **1·BM12** (b). (c, d) POM textures of solvent-free films of **1·BM11** (c) and **1·BM12** (d) prepared by slow evaporation of cyclohexane solutions ($c = 5.0 \times 10^{-3}$ M). (e, f) XRD patterns of the dried films of **1·BM11** (e) and **1·BM12** (f).

tion of the tapelike supramolecular polymers via multipoint $\pi-\pi$ stacking interactions. FE-SEM images of a spin-coated gel displayed fused globular microstructures (Figure 8d). Similar microscopic structures have been reported for lamellarly organized organogels.[36] AFM measurement of the surface of the globular objects visualizes anisotropically aligned fibrous motif with average width of 45 nm (inset in Figure 8d), further confirming the anisotropic orientation of the polymeric species. XRD showed the formation of lamellar structures identical with that of the film prepared from the homogeneous (nongelled) supramolecular polymer solution (Figure 7f). From these results it can be concluded that supramolecular polymers of **1·BM10** have a tendency to organize into continuous lamellar networks.

Folded Supramolecular Polymers. When the number of carbon atoms in the linker moiety reaches 11 (**BM11**) and 12 (**BM12**), their complexes with **1** begin to exhibit properties indicating further elongated polymeric structures. The average hydrodynamic diameters in DLS analysis reached at around 100 nm even in the micromolar regime ($c = 2 \times 10^{-4}$ M, Figure 2). AFM images of the spin-coated solutions on highly oriented pyrolytic graphite (HOPG) revealed existence of well-developed fibrous assemblies with width of 20−50 nm (Figure 9a,b). The persistent length of the assemblies in the AFM images undoubtedly exceeds several micrometers, which is 1 order of magnitude larger than the hydrodynamic diameters measured by DLS (ca. 100 nm) before spin-coating. The large discrepancy between the size regimes of the two techniques is presumably due to high polymerizing propensity of these assemblies, allowing the growth of the polymeric chains during fast evaporation process by spin-coating.

Increasing the concentration of these assemblies eventually leads to the formation of abirefringent viscoelastic gels at around 1.6×10^{-2} M.[14b] FE-SEM observation revealed that the gels are composed of fibers with a uniform diameter of ca. 100 nm (Figure S13). The gel formation is a fast process: they are immediately formed when the homogeneous hot solutions are cooled to ambient temperature. The lack of birefringence and fast gelation as well as considerably high minimum gelation concentrations for these assemblies is markedly contrasting with the lamellar organization of **1·BM10** (birefringent gel is formed even at 2.0×10^{-3} M by prolonged aging) and is a strong indication for the occurrence of different types of self-organization.

Anisotropic orientation of these polymeric assemblies can be achieved by slow evaporation (48 h) of cyclohexane, exhibiting unique stripe textures as shown in Figure 9c,d. A similar texture has been reported for the helically wound supramolecular polymers consisting of a hydrogen-bonded supramolecular polymer[13a] and a Janus-type merocyanine dimer.[4f,37] XRD patterns of these films are characterized by weak and broad reflections emerging at 23.4 Å for **1·BM11**[38] and 26.0 Å for **1·BM12** (Figure 9e,f), respectively, the positions of which are inconsistent with the layer spacings of the lamellar structures obtained from **1·BM8**−**1·BM10**. These distances are close to the intercolumnar distances of the columnar structures obtained from **1·BM5** and **1·BM7** (see Table 2). The formation of columnar structures from a quasi-one-dimensional supramolecular polymer indicates that the polymeric chains of **1·BM11** and **1·BM12** fold into columnar secondary structures.[39,40]

The line broadening of the XRD peaks remained unchanged upon thermal annealing up to 120 °C. This suggests that columns lack a definite long-range lateral positional order as in the nematic columnar (N_c) mesophase.[41] Since the folded polymers can self-assemble weakly through van der Waals interaction between their exterior alkyl chains, they might be able to align anisotropically only in the absence of solvent molecules. The

(36) (a) Jung, J. H.; Ono, Y.; Sakurai, K.; Sano, M.; Shinkai, S. *J. Am. Chem. Soc.* **2000**, *122*, 8648−8653. (b) Ajayaghosh, A.; Varghese, R.; Mahesh, S.; Praveen, V. K. *Angew. Chem., Int. Ed.* **2006**, *45*, 7729−7732. (c) Kumar, N. S. S.; Varghese, S.; Narayan, G.; Das, S. *Angew. Chem., Int. Ed.* **2006**, *45*, 6317−6321.

(37) Yao, S.; Beginn, U.; Gress, T.; Lysetska, M.; Würthner, F. *J. Am. Chem. Soc.* **2004**, *126*, 8336−8348.

(38) For **1·BM11**, an additional peak was observed at 14.8 Å, which does not correspond to either Col_h (13.5 Å) or Col_t (16.5 Å).

(39) (a) Gellman, S. H. *Acc. Chem. Res.* **1998**, *31*, 173−180. (b) Hirschberg, J. H. K. K.; Brunsveld, L.; Ramzi, A.; Vekemans, J. A. J. M.; Sijbesma, R. P.; Meijer, E. W. *Nature* **2000**, *407*, 167−170. (c) Hill, D. J.; Mio, M. J.; Prince, R. B.; Hughes, T. S.; Moore, J. S. *Chem. Rev.* **2001**, *101*, 3893−4011. (d) Hirschberg, J. H. K. K.; Koevoets, R. A.; Sijbesma, R. P.; Meijer, E. W. *Chem.—Eur. J.* **2003**, *9*, 4222−4231.

(40) In our previous study, folding of supramolecular polymer chain was proposed for **1·BM12** from the UV/Vis study: the mixture showed a concentration-independent blue-shifted absorption band of **1** ($\lambda_{max} = 435$ nm) above 2.5×10^{-4} M (see refs 14b and 30b). The formation of H-type aggregates even in micromolar regime clearly demonstrates the intrachain stacking of **1**. In the present study, we found that **1·BM11** also shows similar H-aggregated band ($\lambda_{max} = 440$ nm; see Table 1 and Figure S8) under the same concentration regime. In contrast, the formation of H-type aggregates is not observed for the columnar organization of the discrete 1 + 1 complexes of **1·BM5**−**1·BM7** where the disks can rotate freely around the column axis. For the folded supramolecular polymers of **1·BM11**/**12**, rotational freedom of the constituent disks is restricted by the covalent linkers, and thereby the transition dipole moments of **1** within a column are locked in a specific orientation causing H-type exciton coupling.

(41) (a) Ringsdorf, H.; Wuestefeld, R.; Zerta, E.; Ebert, M.; Wendorff, J. H. *Angew. Chem., Int. Ed.* **1989**, *28*, 914−918. (b) Praefcke, K.; Singer, D.; Kohne, B.; Ebert, M.; Liebmann, A.; Wendorff, J. H. *Liq. Cryst.* **1991**, *10*, 147−159. (c) Kouwer, P. H. J.; Jager, W. F.; Mijs, W. J.; Picken, S. J. *Macromolecules* **2000**, *33*, 4336−4342.

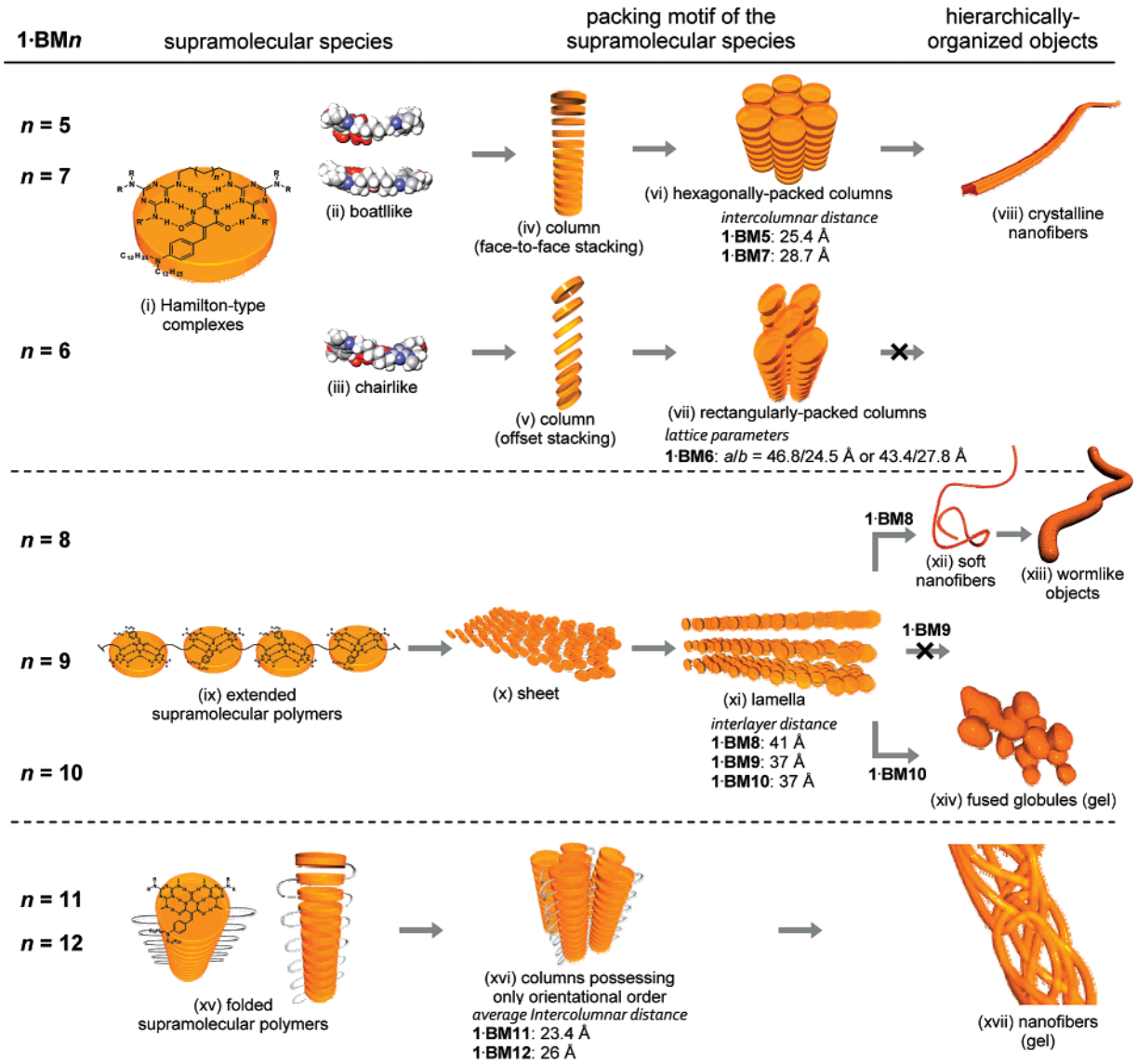

Figure 10. Schematic representation of the hierarchical organization of **1·BM*n***.

folded polymeric assemblies of **1·BM11** and **1·BM12** melt at 144 °C ($\Delta H = 6.4$ kJ mol^{-1}) and 151 °C ($\Delta H = 30.3$ kJ mol^{-1}), respectively, which are the highest values among the investigated assemblies. Interestingly, careful observation of the POM texture of **1·BM11** upon heating unveiled the formation of birefringent fluid phase just before melting. The DSC thermogram indeed showed definite endothermic peak at 131 °C with $\Delta H = 10.1$ kJ mol^{-1}. Thus, it is strongly suggested that **1·BM11** forms columnar mesophase lacking well-defined two-dimensional order in a very narrow temperature range. On the other hand, no such indication was observed for **1·BM12**. The discrepancy in the generation of liquid crystallinity of these assemblies despite their analogous organization behavior remains unclear. **1·BM11** entered liquid crystalline phase at 125 °C and crystallized at 112 °C upon cooling, whereas **1·BM12** directly crystallized at 140 °C.

Summary of Diversifying Superstructures. The results above demonstrate how seemingly minor variations in bismelamines can have a tremendous impact on the resulting self-assembled superstructures containing dye **1**. Hierarchical organization of the assemblies obtained by the aggregation of **1** with **BM*n*** via complementary triple hydrogen-bonding interaction is summarized in Figure 10. At the beginning, diversification occurs in the morphology of the hydrogen-bonded supramolecular species. In the cases of shorter linker bismelamines ($n = 5-7$), stable 1 + 1 complexes are formed upon binding with **1** (i), which hierarchically organize into columnar structures with long-range structural orderings (iv−vii). XRD and POM as well as UV/vis and fluorescence studies revealed, however, that the packing arrangement of these complexes is quite different between $n = 5/7$ and 6, which also has drastic implications for their solution-phase organizations. Dense hexagonal columnar packing of **1·BM5** and **1·BM7** resulted in the formation of crystalline nanofibers with submillimeter length (viii). On the contrary, loose rectangular columnar packing of **1·BM6** failed to form any discrete nanoobjects from solution phase due to its high solubility. From the molecular modeling, it is suggested that the different packing arrangement is a result of the geometrical difference of the 1 + 1 complexes imposed by the odd/even effect of the alkyl linkers (ii and iii). It is quite appealing that the emission property of **1** can be also tuned in addition to the chromophore packing arrangement.

Elongation of the linker length up to $n = 8$ abruptly changes the morphology of the hydrogen-bonded species to extended

supramolecular polymers (ix) organizing into lamellar superstructures (xi) via the formation of two-dimensional sheets (x). This holds true for $n = 9$ and 10. Also, in these cases, the diversification occurs in the highest organization level as represented by the formation of wormlike objects consisting of bundled soft nanofibrils ($n = 8$, xii and xiii) and continuous globular networks ($n = 10$, xiv) in solution phase. The formation of different supramolecular objects is considered to be a consequence of the difference in the rigidity of the extended supramolecular polymers. The formation of more rigid supramolecular polymers in the case of $n = 8$ is self-evident, causing more frustrated packing in the two-dimensional sheets and preventing continuous lateral stacking of the supramolecular polymer networks. In the case of $n = 9$, no hierarchical organization occurs in the solution phase most likely due to the formation of a $1 + 1$ complex as inferred from the DLS study.

Further extension of the linker length up to $n = 11$ and 12 allows supramolecular polymeric chains to be folded into columnar secondary structures (xv) capable of forming viscoelastic gels (xvii). These columnar structures consist of stacked melamine·**1**·melamine hydrogen-bonded segments as the columns of **1·BM5**−**1·BM7** do, but here the disks are connected with upper and lower ones by covalent linkers. This restricts rotational freedom of the disks around the column axis, and thereby their ideal crystalline packing within the columns might be lost. As a result, columns are frustrated in shape and that is why they show only orientational order as demonstrated by XRD.

Conclusions

This study has demonstrated a powerful strategy for the diversification of self-organized architectures of dye-containing self-assemblies. The systematic variation of the non-dye components induces variation of the self-organized superstructures. The notable feature here is that a remarkably simple variation on the linker carbon number of the non-dye component results in dramatic changes in the self-organized superstructures via hydrogen-bond-directed complexation and subsequent hierarchical organization. Thus, one can expect that various self-organized superstructures possessing specific material morphologies including organogels, discrete nanoobjects, and liquid crystals can be obtained from a specifically designed dye without any synthetic alterations. The expression of various materials morphologies may find new function and application of the dye. Furthermore, investigation of the optical and electronic properties of the dyes embedded in such diversified superstructures should bring a deeper understanding of structure−property relationship in exploring organic optoelectronic devices. Our current research effort is focused on the application of this unique strategy to obtain diverse self-organized structures from optically and electronically active π-electronic molecules such as oligothiophenes and perylene bisimides.

Acknowledgment. We are grateful to Dr. Jonathan P. Hill of Organic Nanomaterials Center, NIMS, Tsukuba, Japan, for helpful discussions and Ms. Kanako Unoike of Chiba University for the AFM measurement and to the reviewers of this manuscript for their valuable suggestions on revising the paper. S.Y. thanks The Asahi Glass Foundation for support.

Supporting Information Available: Characterization data for **BM*n***, detailed experimental procedures, and additional microscopic and spectroscopic data for the assemblies. This material is available free of charge via the Internet at http://pubs.acs.org.

JA075257C